Temperature-Dependent Reversible Morphological Transformations in *N*-Oleoyl β-D-Galactopyranosylamine

*Mai Johnson,[‡] Ahanjit Bhattacharya,[‡] Roberto J. Brea, Kira A. Podolsky, and Neal K. Devaraj**

[†]Department of Chemistry and Biochemistry, University of California, San Diego, La Jolla, California 92093, United States.

ABSTRACT

Amphiphilic molecules self-assemble into supramolecular structures of various sizes and morphologies depending on their molecular packing and external factors. Transformations between various self-assembled morphologies is a matter of great fundamental interest. Recently, we reported the discovery of a novel class of single-chain galactopyranosylamide amphiphiles that self-assemble to form vesicles in water. Here, we describe how the vesicles composed of the amphiphile *N*-oleoyl β-D-galactopyranosylamine (**GOA**) undergo a morphological transition to fibers consisting of mainly flat sheet-like structures. Moreover, we show that this transformation is reversible in a temperature-dependent manner. We used several optical microscopy and electron microscopy techniques, circular dichroism spectroscopy, small-angle X-ray scattering, and differential scanning calorimetry, to fully investigate and characterize the morphological transformations of **GOA** and provide a structural basis for such phenomena. These studies provide significant molecular insight into the structural polymorphism of sugar-based amphiphiles and foresee future applications in rational design of self-assembled materials.

INTRODUCTION

Self-assembled organic nanostructures are currently being investigated for use in hydrogel scaffolds,[1,2] sustained drug release applications,[3,4,5] and artificial cell compartments.[6] This bottom-up approach, in which the molecules arrange themselves into organized structures in the absence of external manipulation, is attractive due to their ease of fabrication, and wide diversity of available architectures. Furthermore, the ability to self-reproduce is important for mimicking the studies of a minimal cell and the origins of life. [7,8]

To achieve basic functions such as motility, communication, feeding, growth, and division, living cells rely on self-organizing properties of their membrane components.[9] Cellular membranes are derived from the self-assembly of various amphiphilic lipids. These lipids consist of a nonpolar hydrocarbon tail region, and a polar head group. Depending on the molecular geometry and nature of the functional groups, the lipids can self-assemble in water to form well-defined structures such as micelles, vesicles, fibers, tubules, helical ribbons, and bicontinuous networks.[10] These morphological variations can often be achieved by modifying the polar head groups and lipid tails. Typically, amphiphiles having a cylindrical molecular geometry self-assemble into vesicles. Vesicles are perhaps the closest mimic of the plasma membrane-bound architecture of a living cell and have been used extensively as a scaffold for artificial cell design,[11] microreactor,[6] and drug delivery vehicle.[12] On the other hand, amphiphiles which form tubular or other high-aspect ratio supramolecular structures typically have at least one chiral center, a rigid hydrophobic segment and are capable of forming extended intermolecular hydrogen bonding, which in combination imposes preferential molecular orientation.[13] Examples of these include diacetylenic lipids[14] and surfactants derived from amino acids,[15] sugars,[16] peptides,[17] and bile salts.[18] The ability of these structures to enable spatially and temporally

controlled release of cargo biomolecules, triggered by external inputs such as pH, temperature, or ionic strength, has also made them suitable candidates for the smart delivery of bioactive molecules.[19,20,21] In addition, lipid nanotubes have been used for helical crystallization of proteins.[22]

Interconversion between various supramolecular morphologies in response to external stimuli has been extensively documented in the literature. Transformations between lipidic structures such as lamellar to cubic,[23] and lamellar to inverted hexagonal[24] are well studied in biology and believed to be central to various physiological processes and even pathological states. Several works have reported the transformation between vesicles and various tubular and other high aspect ratio morphologies in response to temperature,[14,25] metal-ion binding,[26,27] and mechanical interventions.[28,29] Among the single-chain amphiphiles (SCAs), those bearing a glucose head group are perhaps the most well-studied for temperature dependent transformations.[30–32] Similar observations were reported for galactose-containing bolaamphiphiles.[33] However, studies of morphological transformations involving galactose-bearing simple SCAs are underrepresented in the literature.

Recently, we reported the discovery of a series of galactose-bearing SCAs that can spontaneously self-assemble to form lamellar membrane-bound vesicles in water.[34,35] Among these self-assembling glycolipids, the *N*-oleoyl β-D-galactopyranosylamine (**GOA**) (Figure 1, Scheme S1 and Figure S1) forms robust bilayer membranes over a wide range of concentrations and is capable of encapsulating biologically relevant molecules. More recently, we reported the formation of stable sponge phase droplets from **GOA** in presence of octylphenoxypolyethoxyethanol surfactants.[36]

We demonstrated that the **GOA** vesicles transition into fibers consisting of flat sheets and needle-like structures upon cooling (Figure 1). Furthermore, **GOA** vesicles regenerated upon heating of the fibers. This reversible morphological transformation between vesicles and fibers provide important insight into the structural formations and adaptability of the galactose-bearing SCAs.

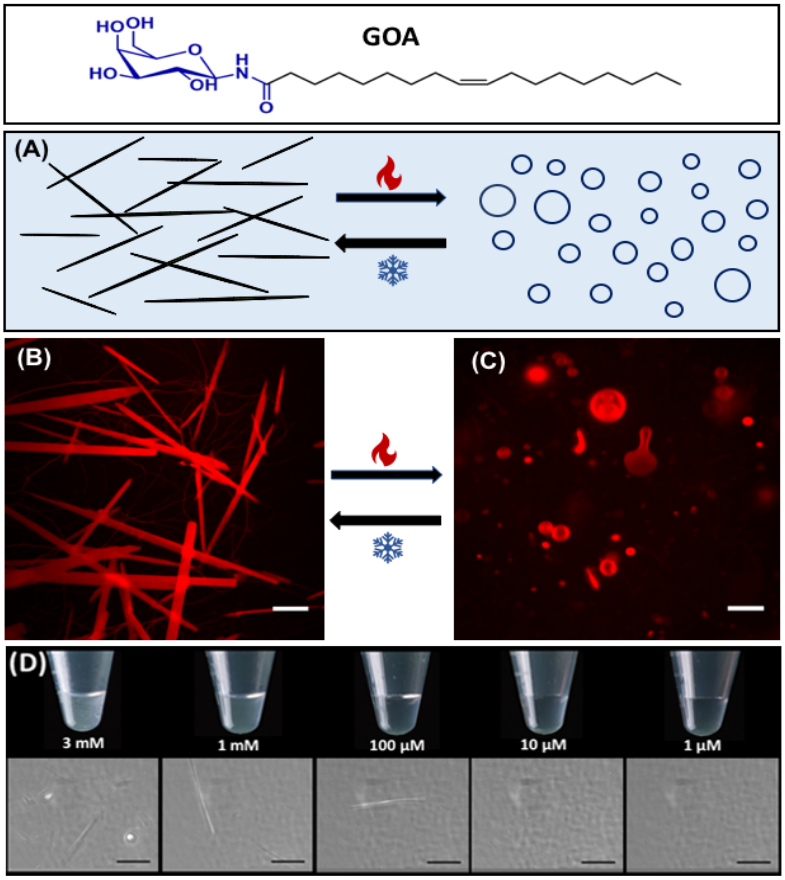

Figure 1. Temperature-dependent morphological transformations of **GOA**. (A) Schematic representation of temperature-dependent reversible fiber-to-vesicle transition of **GOA**. The structure of **GOA** is shown in inset. Spinning-disk confocal microscopy of **GOA**. (B) Fibers existing at room temperature and (C) vesicles when the same fibers are heated significantly above room temperature. The samples were stained with Nile Red. (D) Concentration-dependent formation of **GOA** fiber structures. Fiber formation was not observed below 100 μ**M.** Scale bars represent 10 μm.

EXPERIMENTAL SECTION

Chemicals and materials: Commercially available β-D-galactopyranosylamine was obtained from Toronto Research Chemicals. Oleic acid (OA), O-(7-azabenzotriazol-1-yl)-1,1,3,3-tetramethyl-uronium hexafluorophosphate (HATU), *N*,*N*-dimethylformamide (DMF), *N*,*N*-diisopropylethylamine (DIPEA), chloroform, and Nile Red were obtained from Sigma-Aldrich. Deuterated methanol (CD_3OD) was obtained from Cambridge Isotope Laboratories. HPLC analysis was carried out on an Eclipse Plus C8 analytical column with *Phase A*/*Phase B* gradients [*Phase A*: H_2O with 0.1% formic acid; *Phase B*: MeOH with 0.1% formic acid]. HPLC purification was carried out on Zorbax SB-C18 semipreparative column with *Phase A*/*Phase B* gradients [*Phase A*: H_2O with 0.1% formic acid; *Phase B*: MeOH with 0.1% formic acid]. Nuclear magnetic resonance (^1H NMR) spectra were recorded on a Varian VX-500 MHz spectrometer. Electrospray Ionization-Time of Flight (ESI-TOF) spectra were obtained on an Agilent 6230 Accurate-Mass TOF-MS mass spectrometer. Transmission electron microscopy (TEM) images were recorded on a FEI Tecnai™ Spirit G2 120 kV microscope. Circular dichroism (CD) spectra were recorded on an Aviv CD Spectrometer. Differential scanning calorimetry (DSC) measurements were carried out on a Microcal VP-Capillary DSC instrument (Ward Lab, The Scripps Research Institute). Microscopy was carried out using an Olympus BX51 optical microscope and a Carl Zeiss Axio Observer Z1 spinning-disk confocal microscope.

Synthesis of *N*-oleoyl β-D-galactopyranosylamine (GOA). GOA was synthesized according to Scheme S1. A solution of oleic acid (12.9 mg, 45.8 μmol) in DMF (458 μL) was stirred at 0 ºC for 10 min, and then HATU (19.2 mg, 50.4 μmol) and DIPEA (8.8 μL, 50.4 μmol) were

successively added. After 10 min stirring at 0 ºC, β-D-galactopyranosylamine (8.2 mg, 45.8 μmol) was added. After 1 h stirring at rt, the mixture was concentrated *in vacuo*. The corresponding residue was dissolved in MeOH (250 μL), filtered and purified by HPLC, affording 15.8 mg of **GOA** as a white solid [78%, t_R = 6.8 min (Zorbax SB-C18 semipreparative column, 5% *Phase A* in *Phase B*, 15.5 min)]. ^{1}H NMR (CD_3OD, 500.13 MHz, δ): 5.44-5.25 (m, 2H, 2 × CH), 4.84-4.83 (m, 1H, 1 × CH), 3.88 (d, *J* = 3.1 Hz, 1H, 1 × CH), 3.74-3.63 (m, 2H, 2 × CH), 3.61-3.47 (m, 3H, 1 × CH + 1 × CH_2), 2.34-2.16 (m, 2H, 1 × CH_2), 2.13-1.91 (m, 4H, 2 × CH_2), 1.69-1.55 (m, 2H, 1 × CH_2), 1.41-1.24 (m, 20H, 10 × CH_2), 0.90 (t, *J* = 6.8 Hz, 3H, 1 × CH_3). ^{13}C NMR (CD_3OD, 125.77 MHz, δ): 177.3, 130.9, 130.8, 81.5, 78.2, 75.8, 71.3, 70.5, 62.5, 37.2, 33.1, 30.9, 30.9, 30.6, 30.5, 30.4, 30.3, 30.3, 30.2, 28.2, 28.1, 26.6, 23.7, 14.4. MS (ESI-TOF) [m/z (%)]: 466 ([M +Na]$^+$, 44), 444 ([MH]$^+$, 100]. HRMS (ESI-TOF) calculated for [$C_{24}H_{45}NO_6Na$] ([M +Na]$^+$) 466.3139, found 466.3139.

Formation of GOA vesicles and fibers. Vesicles were prepared by hydration of **GOA** film was in UltraPure distilled water by vigorous vortexing followed by incubation at 42 ºC for 30 min and tumbling at 37 ºC for 1 h. Fibers were prepared by allowing the vesicles to cool at 4 °C overnight or at room temperature for several days.

Transmission electron microscopy (TEM) studies. 4.8 μL of a 3 mM dispersion of **GOA** (fibers or vesicles) in H_2O was added to formvar-coated Cu grid surface and allowed to sit for ~10 s and the excess solution was blotted into a filter paper The grid was washed with 4.8 μL drops of ultrapure H_2O and subsequently stained with 4.8 μL drops of 2% uranyl acetate. The staining was carried out for ~30 s following which excess stain was blotted with filter paper. The grids were dried in air. After this, samples were imaged by transmission electron microscopy (TEM).

Cryo-electron microscopy (cryo-EM). Fibers were prepared from 3 mM **GOA** as described previously. Immediately before grid preparation, the fiber sample was pipetted onto plasma-cleaned 200-mesh Quantifoil R 2/2 copper grids (Quantifoil). Using a Vitrobot EM grid plunger (FEI), excess buffer was blotted at room temperature and 95% humidity and the grids were plunge-frozen in liquid ethane maintained at about -180 °C. The grids were stored in liquid nitrogen until use. Fiber samples were imaged on a 120 kV Libra TEM (Zeiss) fitted with a 2k×2k charge coupled device (CCD) camera.

Scanning electron microscopy (SEM) studies. A dispersion of **GOA** (0.5 mM) fibers was dropped on a glass slide and placed at -80 ºC to freeze. Samples where then dried under vacuum for 2 h. The freeze-dried samples were sputter coated with 5 nm of iridium prior to imaging at 5 kV on FEI Apreo SEM.

Atomic force microscopy (AFM) studies. A dispersion of GOA fibers (0.5 mM) was drop-coated on a clean Si wafer surface and air-dried. AFM scans were acquired with a multimode Veeco system with nanoscope controller IV in tapping mode. The cantilevers used were HQ:NSC15/AL BS with a resonance frequency of 325 kHz and spring constant 40 N/m. Images were acquired at a scan rate of 0.5 Hz. Images were processed using the software Gwyddion.

Small-angle X-ray scattering (SAXS). SAXS studies were carried out at the beamline 12-ID-C at the Advanced Photon Source (APS), Argonne National Laboratory (ANL). The samples were placed in capillary tubes with 0.01 mm walls and 15 mm outer diameter (15-SG, Charles Supper Company). SAXS measurements were performed with monochromatic photon flux of 1×10^{13} photons s^{-1} cm^{-2}. A 1×1 mm^2 focused beam of incident photon energy at 18 keV (wavelength = 0.69 Å) was used with exposure times of 1 s. The SAXS data were collected by a

CCD detector (2048×2048 pixels) and the sample-to-detector distance was 3825 mm. One-dimensional SAXS profiles were derived by azimuthal averaging of the two-dimensional scattering data with proper background subtraction using the Igor Pro macro Nika. Finally, the scattering intensity profiles were obtained as a function of the scattering vector (q).

Circular dichroism (CD) spectroscopy. CD spectra were recorded on a Jasco J-1500 CD Spectrometer. **GOA** was suspended in deionized water at a concentration of 3.0 mM. Then, 200 μL of the sample was loaded into a quartz cuvette (1 mm light path) and scanned from 260 nm to 190 nm at every 1 nm interval. The sample was measured at 25, 37, and 60 ºC. The background consisted of deionized water and an average of five individual scans were measured. Presented spectra represent averages of ten individual scans with background subtraction.

Differential scanning calorimetry (DSC). DSC measurements were carried out on a Microcal VP-Capillary DSC at the Ward Lab (The Scripps Research Institute). 450 μL of 0.5 mM dispersions of **GOA** in water were used for all experiments. The scan rates were 30 ºC/h and the *gain* were set to "high". Background subtraction and data analyses were carried out using Microcal Origin software as provided by the manufacture.

Real-time microscopy of morphological transformations. Vesicle and fiber samples were prepared from 3 mM **GOA** as described earlier. For observing fiber-to-vesicle transformation, 30 μL of the dispersion was loaded into a 0.20 mm×2.00 mm rectangular borosilicate tube (Vitrocom). The loaded samples were then placed on the Peltier stage (Linkam Scientific Instruments) connected to a water circulating pump and observed with 40X objective on an Olympus BX51 microscope. The temperature was set at 4 to 95 ºC at a rate of 5 ºC/min.

For observation of the vesicle-to-fiber transformation, Vesicle samples were loaded on a micro-insert dish (Ibidi Cat. No. 80486), in a humidified chamber and imaged on the spinning

disk microscopy (Zeiss) at 20X magnification. The images were acquired every 10 min for a total of 96 h.

Cell Culture. Hep3B liver cancer cell lines (ATCC, HB-8064) were cultured at a density of 5×10^4 cells per well in 8-well glass chambers in EMEM media containing L-Glutamine (Quality Biological) supplemented with 10% heat inactivated FBS (Omega Scientific, FB-02), and 1% penicillin/streptomycin (Life Technologies Cat. No. 15140122) for 24 hours in 37 ºC incubator with 5% CO_2. Next day, the media was replaced with 300 μL Opti-MEM media (Life Technologies Cat. No. 31985070). Vesicles were prepared by hydration of 3.21 mM **GOA** film in HBSS and 0.714 mM Tween 80, followed by incubation at 50 ºC for 10 min. Vesicles were then extruded through 0.1 μm polycarbonate membrane using Avanti Mini-Extruder (Avanti Polar Lipids, Inc.), and concentration was obtained by preparing a standard curve on HPLC. 100 μM **GOA** vesicles were added to the well and HBSS (Life Technologies Cat. No. 14175095) was added to another well as control. Cells were then incubated for 4 hours at 37 ºC incubator with 5% CO_2 and imaged on the spinning-disk confocal microscopy (Zeiss) using 20X objective.

RESULTS AND DISCUSSION

Morphological transformation of GOA. Initially, we prepared **GOA** vesicles incorporating 0.1 mol% Nile Red by hydrating a lipid film above 37 °C. The vesicles were then kept below room temperature (typically 4 °C) overnight, and fiber structures of flat sheet and needle-like morphologies were observed by spinning-disk confocal microscopy (Figure 1B). When the fibers were briefly placed in a 95 °C heat block, vesicles were observed only (Figure 1C). In addition to the influence of temperature in the formation of the fibers, the molecular self-assembly also depended on the concentration of **GOA**. At concentrations below 100 μM, fiber formation was not observed (Figure 1D). This observation is in good agreement with our previous study[35] where

we estimated the critical aggregation concentration (cac) of **GOA** for vesicle formation to be approximately 79 μM.

To determine if the solvent (in this case, water) is important in maintaining the sheet-like structures, water was removed by lyophilization. Upon lyophilization, the samples appeared dry and a white powder was formed. Analysis of the resulting material by optical and polarized light microscopy (PLM) showed preferentially the presence of several populations of aggregates as well as fibrous structures (Figure S2). The aggregates observed could be due to loss of hydrogen bonding of the -OH groups of the galactopyranosyl head-groups with water. Further, we observed that the self-assembled structures of **GOA** are not formed in polar organic solvents such as dimethylformamide, dimethyl sulfoxide methanol, and ethanol. Thus, the presence of water is likely to contribute to the stabilization of the **GOA** fibers as previously noted with other amphiphilic systems.[37] We also prepared vesicles from **GOA** in presence of small quantities (6.25 mol%) of Tween 80 in various buffers such as HEPES buffered saline (pH 7.4), Hanks Balance Salt Solution (HBSS), and phosphate buffered saline (pH 7.4) as previously described.[35] Upon incubation of the vesicles below room temperatures, we observed formation of fiber structures.

TEM, SEM, cryo-TEM, and AFM studies. We next characterized the self-assembled structures of **GOA** by TEM, SEM, cryo-TEM, and AFM. Aqueous dispersions of **GOA** vesicles were extruded through a 0.1 μm polycarbonate filter using a hand-held device (Avanti Polar Lipids) and imaged by negative-staining TEM. Representative TEM images of the vesicular architectures showed average diameter to be about 130 nm (Figure 2A). The majority of the sample exhibited flat sheet-like structures (Figure 2B) although needle like structures were also observed (Figure 2C). The average width of the needle-like structures was approximately 60 nm,

measuring around 2 μm in length. The flat sheet-like structures are much larger with an average width of 900 nm and approximately 9 μm in length. Additional examination of the fiber structures by SEM and cryo-TEM reconfirmed the presence of flat sheet-like structures with smooth surface morphology and needle-like structures with pointed ends (Figures 2D, 2E, and 2F).

AFM studies were also carried out to estimate the 3D height distributions of different fiber structures. We observed that the flat sheets have heights in the range of about 50-200 nm while the needle-like structures have heights in the range of about 30-120 nm (Figure S3).

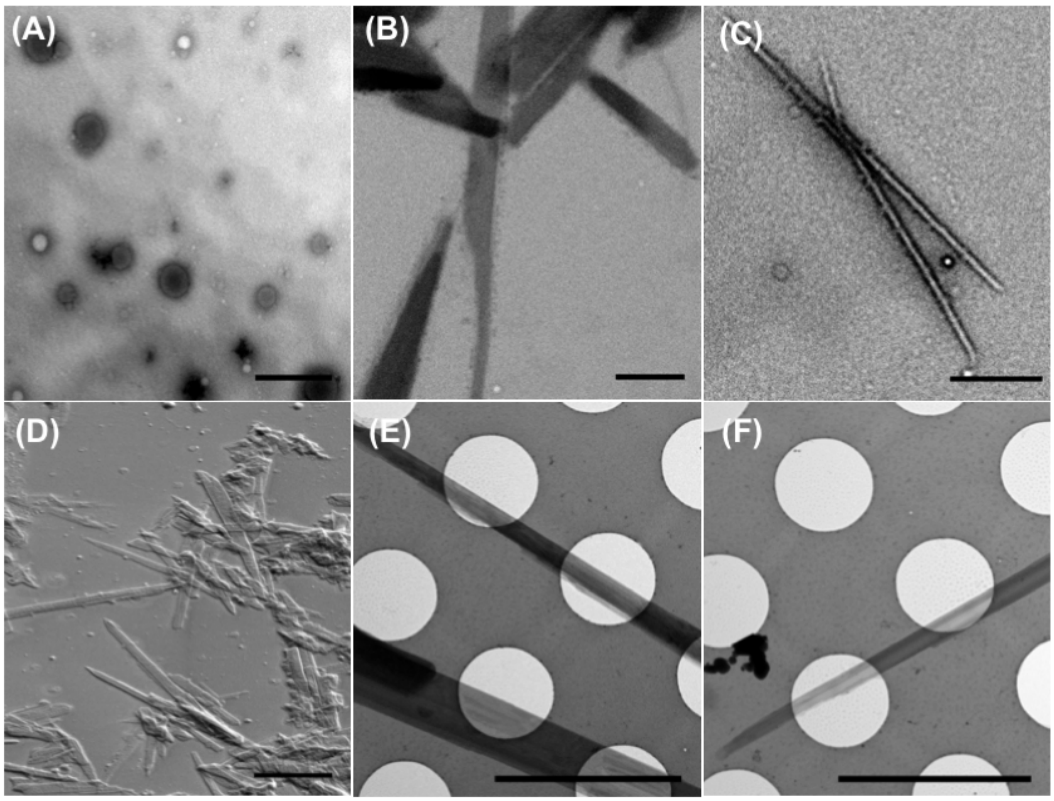

Figure 2. Electron microscopy characterization of the self-assembled structures of **GOA**. Negative staining TEM images confirming the formation of vesicles (A), flat sheets (B) and needle-like structures (C). Scale bars: A – 500 nm, B – 500 nm, C – 1.5 μm. (D) SEM images of fiber samples. Scale bar denotes 5 μm. Cryo-TEM images of flat sheet (E) and needle-like structures (F). Scale bars represent 5 μm.

GOA fibers exhibit long-range structural order and chiral packing. Once we studied the self-assembled structures of **GOA** by microscopy, we sought to determine if the fibers presented any long-range order in their supramolecular structure. PLM revealed that the fibers exhibited birefringence (Figure 3A). This is indicative of the presence of anisotropy and long-range order in the overall structure. In comparison, a dispersion of vesicles did not exhibit any birefringence, suggesting that they are isotropic in organization (Figure 3B).

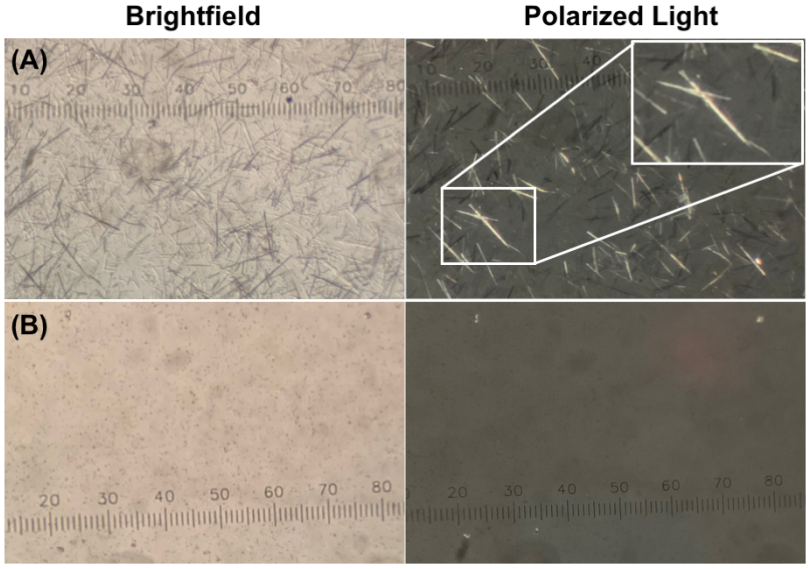

Figure 3. Polarized light microscopy (PLM) of **GOA** samples. (A) Bright field (*left*) and polarized light (*right*) micrographs of a fiber dispersion exhibiting birefringence (A), vesicle dispersion exhibiting no birefringence (B). Both samples are prepared from 3 mM **GOA**.

Next, we investigated if the self-assembly of the fibers exhibit any chiral packing of the constituent amphiphilic monomers. Circular dichroism (CD) spectroscopy can provide experimental evidence that formation of fibers is directed by chiral molecular packing.[14] At 25 °C, CD spectrum of the **GOA** sample containing fiber-like structures showed a negative peak centered approximately at 220 nm (Figure 4). When the temperature of the sample was raised to 37 °C, the CD signal diminished and disappeared at 60 °C. The hydrocarbon chains are packed

in a fluid state at higher temperatures in vesicle morphologies resulting in loss of CD signal. These results indicated the presence of chiral molecular packing in the fiber-like structures but not in the vesicles.

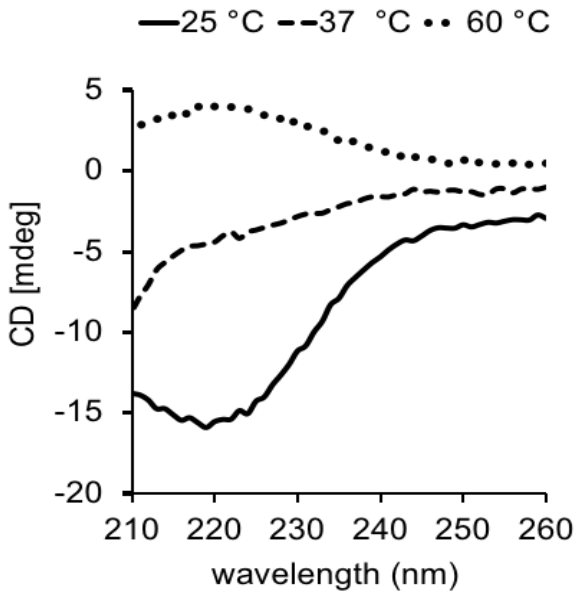

Figure 4. Circular dichroism (CD) spectra of **GOA** dispersions (fibers and vesicles) at varying temperatures.

SAXS measurements. To study the mesophase behavior of the vesicles and fibers, we employed SAXS using synchrotron radiation source. A dispersion of **GOA** fibers loaded in a glass capillary gave Bragg reflections (n = 1, 2), suggesting the presence of lamellar ordering (Figure 5A). From the intensity profile, the d-spacing ($d = 2\pi/q$) was calculated to be 37.40 Å. This distance is slightly higher than the previously calculated head-to-head distance of 35.25 Å (for **GOA** bilayers),[33] suggesting that the **GOA** molecules are only weakly hydrated in the fibers. When the same capillary was heated above main phase transition temperature, Bragg reflections (n = 1, 2) were obtained at higher lamellar repeat distances (Figure 5B) and the intensity was decreased. The d-spacing was calculated to be 45.53 Å, as expected from a more disordered molecular packing in fluid phase vesicular morphology.

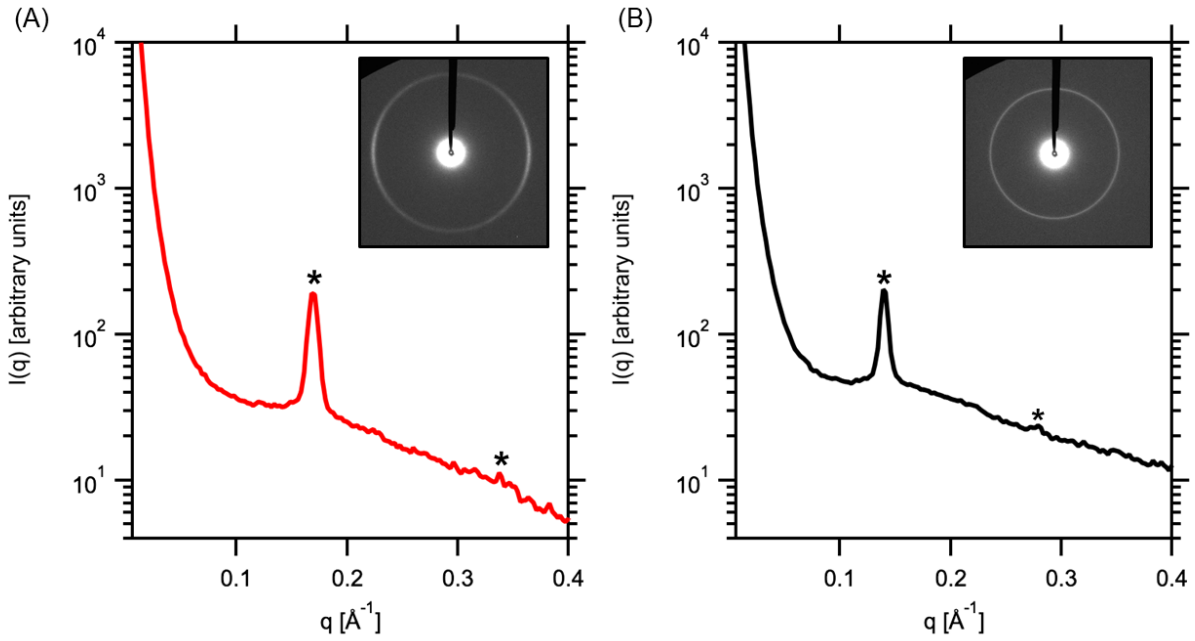

Figure 5. Synchrotron small-angle X-ray scattering (SAXS) studies on **GOA** dispersions. The intensity profiles correspond to fibers (A) and vesicles (B). The Bragg peaks are marked with asterisks. The inset images show the diffraction patterns.

Real-time transition of fibers to vesicles and *vice versa*. To visualize the transition of fibers to vesicles in real-time, the fibers were loaded in a rectangular glass capillary and subjected to a temperature rise from 4 to 95 °C at a rate of 5 °C/min on a temperature-controlled microscope stage. As shown in Figure 6, the number of fibers observed began to decrease with increasing temperature. Vesicles began to appear when the stage temperature reached 50 °C. As the temperature is increased from 70 to 79 °C, vesicle formation along the fibers are clearly visible (Figure 6, Movie S1). Finally, all fibers are converted to vesicles when the stage temperature reached 80 °C and beyond (data not shown). It is important to point out that while the stage temperature can be controlled, the exact temperature inside the glass capillary is likely to be much lower than that of the stage depending on the rate of heat conduction. Therefore, the observed transitions may have taken place at lower temperatures than the set temperature of the

stage. No morphological change was observed when the temperature gradient is reversed at the same rate. The reverse process of vesicle-to-fiber transition is considerably slow, ranging from 10-12 h at 4 °C to several days at room temperature. We followed the transition of vesicles to fibers in a sealed chamber at room temperature by continuous imaging over 4 days (Movie S2).

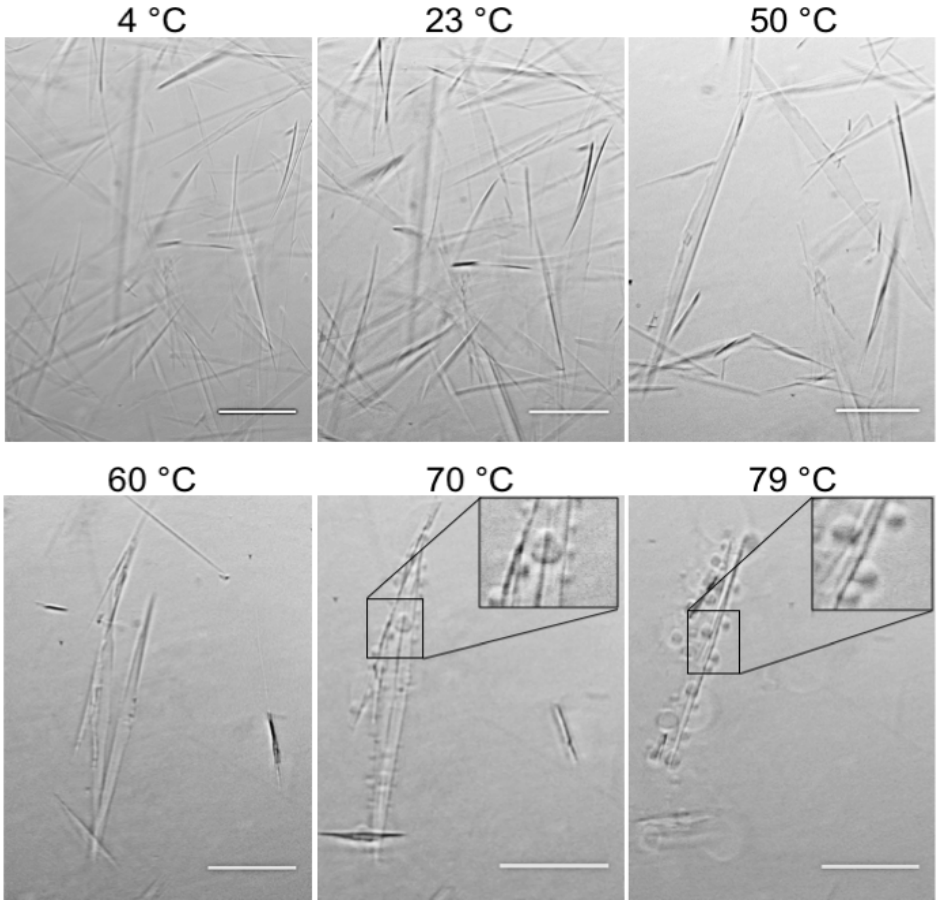

Figure 6. Temperature-induced fiber-to-vesicle transition observed by phase contrast microscopy. The indicated temperatures are those of the temperature-controlled microscopy stage. Vesicles are shown enlarged in inset for clarity. Scale bars denote 50 μm.

DSC measurements. To better understand the transition between fibers and vesicles, we further investigated the thermodynamic nature of this process. We believe that the vesicle-to-fiber transformation is driven by entropy. Thus, increase of temperature facilitates the formation of vesicles, which is the entropically less costly form. Moreover, we observed that duration over

which the samples are incubated at a particular temperature can affect the transition between the two morphologies. To determine the precise temperature range where the morphological changes take place, we employed DSC. In good agreement to our previous report,[35] DSC scans on a multilamellar dispersion of **GOA** revealed the presence of two peaks – an intense, sharp, and symmetrical peak centered at 25 °C, and a broad, strong, asymmetrical peak with maximum at 37 °C (Figure 7A). In this experiment, the sample block was incubated at 4 °C for 10 h. As the holding time is shortened to ~3 h, the first peak is diminished while the second peak remained unchanged (Figure 7B). When the samples were incubated throughout at 25 °C, the first peak disappeared (Figure 7C). Thus, incubation of a multilamellar vesicular dispersion of **GOA** at low temperature for prolonged time showed how the vesicles transformed to fibers *in situ* and displayed the respective DSC peaks. However, when the samples were incubated at higher temperatures, the vesicles partly retained their fluid nature and no conversion to fibers was observed. We further corroborated these results by microscopic observations of the left-over dispersions and observed fibers in the first two conditions, but only vesicles in the final condition. We attributed the peak at 37 °C to be the main transition peak (gel to fluid), and the sharp peak at 25 °C as the one corresponding to the fiber-to-vesicle transition. Based on the sharpness of the DSC peak, we reason that the fiber-to-vesicle transformation is a cooperative process as suggested in previous reports.[38]

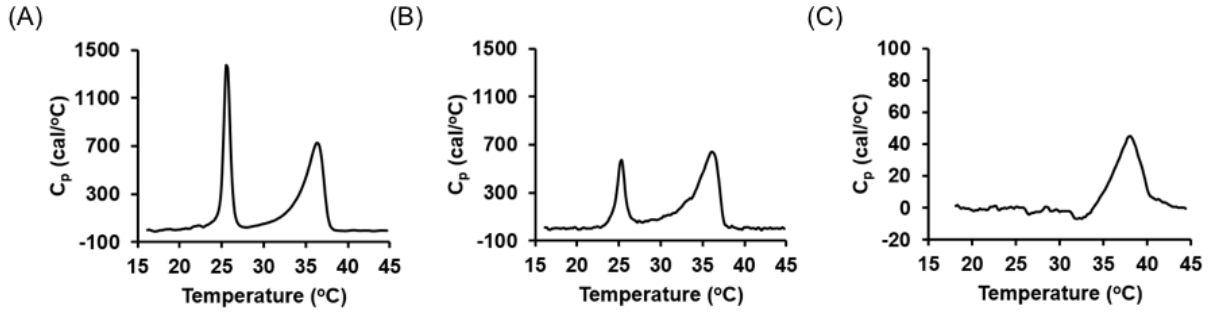

Figure 7. Differential scanning calorimetry (DSC) of **GOA** samples under various conditions. DSC scans revealed a sharp peak at 25 °C when 0.5 mM aqueous dispersions of **GOA** were incubated at 4 °C for longer (9-10 h) duration (A) and shorter (2-3 h) duration (B). Alternatively, incubation of the samples at 25 °C only showed a single broad peak (C).

CONCLUSION

We have shown that the single-chain amphiphile **GOA** can transition between two different morphologies in a temperature-dependent manner. On a molecular level, we believe that strong directional intermolecular interactions among the amide groups near the head-group region play a key role in the transformation between vesicles to fibrous structures similar to what has been reported with other amphiphilic systems.[33,39] Interestingly, we observed that vesicles derived from *S*-oleoyl β-D-thiogalactopyranose (**OTG**)[34] do not transform to fibers even after one week of incubation at 4 °C, further highlighting the significance of the amide bond for such transformation to take place.

In the context of possible drug delivery applications, it would be important to take into consideration the biocompatibility of the self-assembly of the amphiphiles.[40] Though the chemical functional groups in **GOA** are compatible with biomolecules, the formation of the fiber structures may influence cell viability through physical interactions. Preliminary studies on Hep3B cells showed that fibers and needle-like structures formed from **GOA** vesicles added to cell culture media resulted in cell death (SI, page S5, Figure S4). The cell death is likely due to the physical contact of the fibers with the cell membrane.

In summary, these studies provide new insight into the morphological transitions of the single-chain amphiphile **GOA**. The transition from vesicles to fibers/sheet-like structures and the reverse transformation is mainly influenced by temperature. Future studies will be necessary to

analyze the effects of alternate sugar headgroups, such as fucose, mannose, or xylose. Morphological transitions dependent on physical factors may find application in membrane mimetic studies and shape transformations in protocells.

AUTHOR INFORMATION

Corresponding Author

*Email: ndevaraj@ucsd.edu

ORCID

Mai Johnson: 0000-0002-6026-8821

Ahanjit Bhattacharya: 0000-0001-6810-9537

Roberto J. Brea: 0000-0002-0321-0156

Kira A. Podolsky: 0000-0003-3152-6593

Neal K. Devaraj: 0000-0002-8033-9973

Author Contributions

The manuscript was written through contributions of all authors. All authors have given approval to the final version of the manuscript. ‡These authors contributed equally.

Notes

The authors declare no competing financial interest.

ASSOCIATED CONTENT

Supporting Information

The Supporting Information is available free of charge on the ACS Publications website.

NMR spectral images, Scheme S1, Figure S1, Figure S2, Figure S3 (PDF)

Movies S1 and S2 (AVI)

ACKNOWLEDGMENT

This work is in part supported by the National Science Foundation (CHE-1844346), the National Institutes of Health (DP2DK111801-01S2 and T32CA009523-33), Young Investigator Grant from the Human Frontier Science Research Program (RGY0066/2017) and the U.S. Department of Energy (Biomolecular Materials Program, Division of Materials Sciences and Engineering). We thank Soenke Seifert (Advanced Photon Source, Argonne National Laboratory) and Sudip Pandey (UC San Diego) for technical guidance during Synchotron SAXS experiments and Prof. Sunil K. Sinha (UC San Diego) for interpretation of the data. We thank Marcus Jager and Christian M. Cole (Kelly Lab, The Scripps Research Institute) for their assistance and suggestions with CD Spectroscopy. We thank Gabriel Ozorowski (Ward Lab, The Scripps Research Institute) for collaboration with Differential Scanning Calorimetry. We acknowledge the use of the UCSD Cryo-Electron Microscopy Facility, which is supported by NIH grants to Timothy S. Baker and a gift from the Agouron Institute to UCSD. This work was supported by the Waitt Advanced Biophotonics Core Facility of the Salk Institute (NIH-NCI CCSG: P30 014195) and the Waitt Foundation.

REFERENCES

(1) Guo, Y.; Yui, H.; Minamikawa, H.; Yang, B.; Masuda, M.; Ito, K.; Shimizu, T. Dimension Control of Glycolipid Nanotubes by Successive Use of Vesicle Extrusion and Porous Template. *Chem. Mater.* **2006**, *18*, 1577–1580.

(2) Fu, I. W.; Nguyen, H. D. Sequence-Dependent Structural Stability of Self-Assembled Cylindrical Nanofibers by Peptide Amphiphiles. *Biomacromolecules* **2015**, *16*, 2209–2219.

(3) Lin, M. S.; Chen, R. T.; Yu, N. Y.; Sun, L. C.; Liu, Y.; Cui, C. H.; Xie, S. Y.; Huang, R. Bin; Zheng, L. S. Fullerene-Based Amino Acid Ester Chlorides Self-Assembled as Spherical Nano-Vesicles for Drug Delayed Release. *Colloids Surfaces B Biointerfaces* **2017**, *159*, 613-619.

(4) Matson, J. B.; Stupp, S. I. Self-Assembling Peptide Scaffolds for Regenerative Medicine. *Chem. Commun.* **2012**, *48*, 26-33.

(5) Blanazs, A.; Armes, S. P.; Ryan, A. J. Self-Assembled Block Copolymer Aggregates: From Micelles to Vesicles and Their Biological Applications. *Macromolecular Rapid Communications*. 2009, *30*, 267-277.

(6) Buddingh', B. C.; Van Hest, J. C. M. Artificial Cells: Synthetic Compartments with Life-like Functionality and Adaptivity. *Acc. Chem. Res.* **2017**, *50*, 769–777.

(7) Exterkate, M.; Driessen, A. J. M. Synthetic Minimal Cell: Self-Reproduction of the Boundary Layer. *ACS Omega* **2019**, *4*, 5293-5303.

(8) Banerjee, P.; Pal, S.; Kundu, N.; Mondal, D.; Sarkar, N. A Cell-Penetrating Peptide Induces the Self-Reproduction of Phospholipid Vesicles: Understanding the Role of the Bilayer Rigidity. *Chem. Commun.* **2018**, *54*, 11451-11454.

(9) Van Meer, G.; Voelker, D. R.; Feigenson, G. W. Membrane Lipids: Where They Are and How They Behave. *Nat. Rev. Mol. Cell Biol.* **2008**, *9*, 112–124.

(10) Lipowsky, R. The Conformation of Membranes. *Nature* **1991**, *349*, 475–481.

(11) Bhattacharya, A.; Brea, R. J.; Devaraj, N. K. De Novo Vesicle Formation and Growth: An Integrative Approach to Artificial Cells. *Chem. Sci.* **2017**, *8*, 7912–7922.

(12) Li, J.; Wang, X.; Zhang, T.; Wang, C.; Huang, Z.; Luo, X.; Deng, Y. A Review on Phospholipids and Their Main Applications in Drug Delivery Systems. *Asian J. Pharm.*

Sci. **2014**, *10*, 81–98.

(13) Shimizu, T.; Masuda, M.; Minamikawa, H. Supramolecular Nanotube Architectures Based on Amphiphilic Molecules. *Chem. Rev*. **2005**, *105*, 1401-1443.

(14) Schnur, J. M.; Ratna, B. R.; Selinger, J. V.; Singh, A.; Jyothi, G.; Easwaran, K. R. K. Diacetylenic Lipid Tubules: Experimental Evidence for a Chiral Molecular Architecture. *Science*. **1994**, *264*, 945-947.

(15) Brito, R. O.; Oliveira, I. S.; Araújo, M. J.; Marques, E. F. Morphology, Thermal Behavior, and Stability of Self-Assembled Supramolecular Tubules from Lysine-Based Surfactants. *J. Phys. Chem. B* **2013**, *117*, 9400-9411.

(16) Hato, M.; Minamikawa, H.; Tamada, K.; Baba, T.; Tanabe, Y. Self-Assembly of Synthetic Glycolipid/Water Systems. *Adv. Colloid Interface Sci*. **1999**, *80*, 233–270.

(17) Zhao, Y.; Yang, W.; Wang, D.; Wang, J.; Li, Z.; Hu, X.; King, S.; Rogers, S.; Lu, J. R.; Xu, H. Controlling the Diameters of Nanotubes Self-Assembled from Designed Peptide Bolaphiles. *Small* **2018**, *14*, e1703216.

(18) Di Gregorio, M. C.; Severoni, E.; Travaglini, L.; Gubitosi, M.; Sennato, S.; Mura, F.; Redondo-Gómez, C.; Jover, A.; Pavel, N. V.; Galantini, L. Bile Acid Derivative-Based Catanionic Mixtures: Versatile Tools for Superficial Charge Modulation of Supramolecular Lamellae and Nanotubes. *Phys. Chem. Chem. Phys*. **2018**, *20*, 18957-18968.

(19) Ilbasmis-Tamer, S.; Unsal, H.; Tugcu-Demiroz, F.; Kalaycioglu, G. D.; Degim, I. T.; Aydogan, N. Stimuli-Responsive Lipid Nanotubes in Gel Formulations for the Delivery of Doxorubicin. *Colloids Surfaces B Biointerfaces* **2016**, *143*, 406-414.

(20) Chen, J.; Zhang, B.; Xia, F.; Xie, Y.; Jiang, S.; Su, R.; Lu, Y.; Wu, W. Transmembrane

Delivery of Anticancer Drugs through Self-Assembly of Cyclic Peptide Nanotubes. *Nanoscale* **2016**, *8*, 7127-7136.

(21) Fong, W. K.; Hanley, T. L.; Thierry, B.; Kirby, N.; Boyd, B. J. Plasmonic Nanorods Provide Reversible Control over Nanostructure of Self-Assembled Drug Delivery Materials. *Langmuir* **2010**, *26*, 6136-6139.

(22) Wilson-Kubalek, E. M.; Brown, R. E.; Celia, H.; Milligan, R. A. Lipid Nanotubes as Substrates for Helical Crystallization of Macromolecules (Tubules=helical Arrays=galactosylceramides=electron Microscopy). *Biophysics (Oxf)*. **1998**, *95*, 8040–8045.

(23) Almsherqi, Z. A.; Kohlwein, S. D.; Deng, Y. Cubic Membranes: A Legend beyond the Flatland* of Cell Membrane Organization. *J. Cell Biol*. **2006**, *173*, 839–844.

(24) Jouhet, J. Importance of the Hexagonal Lipid Phase in Biological Membrane Organization. *Front. Plant Sci*. **2013**, *4*, 494.

(25) Fujima, T.; Frusawa, H.; Minamikawa, H.; Ito, K.; Shimizu, T. Elastic Precursor of the Transformation from Glycolipid Nanotube to Vesicle. *J. Phys. Condens. Matter* **2006**, *18*, 3089–3096.

(26) Papahadjopoulos, D.; Vail, W. J.; Jacobson, K.; Poste, G. Cochleate Lipid Cylinders: Formation by Fusion of Unilamellar Lipid Vesicles. *BBA - Biomembr*. **1975**, *394*, 483–491.

(27) Ortiz, A.; Killian, J. A.; Verkleij, A. J.; Wilschut, J. Membrane Fusion and the Lamellar-to-Inverted-Hexagonal Phase Transition in Cardiolipin Vesicle Systems Induced by Divalent Cations. *Biophys. J*. **1999**, *77*, 2003–2014.

(28) Heinrich, V.; Božič, B.; Svetina, S.; Žekš, B. Vesicle Deformation by an Axial Load: From Elongated Shapes to Tethered Vesicles. *Biophys. J*. **1999**, *76*, 2056–2071.

(29) Sugihara, K.; Chami, M.; Derényi, I.; Vörös, J.; Zambelli, T. Directed Self-Assembly of Lipid Nanotubes from Inverted Hexagonal Structures. *ACS Nano* **2012**, *6*, 6626–6632.

(30) Kamiya, S.; Minamikawa, H.; Jung, J. H.; Yang, B.; Masuda, M.; Shimizu, T. Molecular Structure of Glucopyranosylamide Lipid and Nanotube Morphology. *Langmuir* **2005**, *21*, 743-750.

(31) Shimizu, T.; Minamikawa, H.; Kogiso, M.; Aoyagi, M.; Kameta, N.; Ding, W.; Masuda, M. Self-Organized Nanotube Materials and Their Application in Bioengineering. *Polym. J.* **2014**, *46*, 831–858.

(32) Kameta, N.; Matsuzawa, T.; Yaoi, K.; Fukuda, J.; Masuda, M. Glycolipid-Based Nanostructures with Thermal-Phase Transition Behavior Functioning as Solubilizers and Refolding Accelerators for Protein Aggregates. *Soft Matter* **2017**, *13*, 3084–3090.

(33) Masuda, M.; Shimizu, T. Lipid Nanotubes and Microtubes: Experimental Evidence for Unsymmetrical Monolayer Membrane Formation from Unsymmetrical Bolaamphiphiles. *Langmuir* **2004**, *20*, 5969–5977.

(34) Brea, R. J.; Bhattacharya, A.; Bhattacharya, R.; Song, J. J.; Sinha, S. K.; Devaraj, N. K. Highly Stable Artificial Cells from Galactopyranose-Derived Single-Chain Amphiphiles. *J. Am. Chem. Soc.* **2018**, *140*, 17356-17360.

(35) Bhattacharya, A.; Brea, R. J.; Song, J. J.; Bhattacharya, R.; Sinha, S. K.; Devaraj, N. K. Single-Chain β-D-Glycopyranosylamides of Unsaturated Fatty Acids: Self-Assembly Properties and Applications to Artificial Cell Development. *J. Phys. Chem. B* **2019**, *123*, 3711–3720.

(36) Bhattacharya, A.; Niederholtmeyer, H.; Podolsky, K. A.; Bhattacharya, R.; Song, J.-J.; Brea, R. J.; Tsai, C.-H.; Sinha, S. K.; Devaraj, N. K. Lipid Sponge Droplets as

Programmable Synthetic Organelles. *bioRxiv* **2020**, *bioRxiv* 2020.01.20.913350.

(37) Yang, B.; Kamiya, S.; Yui, H.; Masuda, M.; Shimizu, T. Effective Shortening in Length of Glycolipid Nanotubes with High Axial Ratios. *Chem. Lett.* **2003**, *32*, 1146–1147.

(38) Smulders, M. M. J.; Nieuwenhuizen, M. M. L.; De Greef, T. F. A.; Van Der Schoot, P.; Schenning, A. P. H. J.; Meijer, E. W. How to Distinguish Isodesmic from Cooperative Supramolecular Polymerisation. *Chem. - A Eur. J.* **2010**, *16*, 362-367.

(39) Jung, J. H.; John, G.; Yoshida, K.; Shimizu, T. Self-Assembling Structures of Long-Chain Phenyl Glucoside Influenced by the Introduction of Double Bonds. *J. Am. Chem. Soc.* **2002**, *124*, 10674–10675.

(40) Tan, A.; Hong, L.; Du, J. D.; Boyd, B. J. Self-Assembled Nanostructured Lipid Systems: Is There a Link between Structure and Cytotoxicity? *Advanced Science*. **2019**, *6*, 1801223.

TOC Graphic